Progress In Electromagnetics Research C, Vol. 82, 225–235, 2018

A Penta-Band Reject Inside Cut Koch Fractal Hexagonal Monopole UWB MIMO Antenna for Portable Devices

Gnanaharan Irene* **and Anbazhagan Rajesh**

Abstract—In this paper, a novel compact hexagonal shaped ultra-wideband multiple-input multiple-output (UWB-MIMO) Koch fractal antenna is designed with penta-band rejection characteristics for portable devices. The antenna rejects the C-band downlink frequency from 3.7–4 GHz, the C-band uplink frequency from 5.75–6.05 GHz and the satellite bands from 7.45 to 8.4 GHz. The band 7.45–7.55 GHz is used by the meteorological satellite service for the geostationary satellite services. The band 7.75–7.9 GHz is used by the meteorological satellite service for non-geostationary satellite services. The band 8.025–8.4 GHz is used by the Earth exploration satellites for geostationary satellite services. The C-band and satellite bands interfere with the UWB and have been rejected using a band reject filter. A spiral shaped slot is introduced inside the fractal hexagonal monopole to introduce band reject characteristics. The band suppression and widening of the impedance bandwidth are achieved by using defected ground structures. The antenna has wideband impedance matching with $S_{11} < -10$ dB in the UWB frequency range from 3.1 to 13.6 GHz and has a low mutual coupling with $S_{21} < -19$ dB. The antenna has very low envelope correlation coefficient of less than 0.17 and low capacity loss of 0.254, which proves that the MIMO antenna shows good diversity performance.

1. INTRODUCTION

In recent years, as the demand for applications using high data rate is increasing, Ultra Wide Band (UWB) is becoming an important area of interest. The main reason considered for UWB technology is its high data rate and low power requirements. Moreover, unlicensed frequency that ranges from 3.1 to 10.6 GHz has been allocated by Federal Communication Commission (FCC). However, the main disadvantages of UWB are its limited channel capacity and short communication. These limitations can be overcome by using Multiple Input Multiple Output (MIMO) technology [1]. The advantages of using MIMO is the increased channel capacity and the overall transmission range for the same power requirements as it uses multiple antennas in the transmitter and receiver sides [2].

Presently, the Wireless Personal Area Network (WPAN) and Wireless Body Area Network (WBAN) use UWB-MIMO technology due to high data rate. However, the main disadvantage of MIMO technology is its large mutual coupling which is introduced due to the presence of multiple antennas [3]. The signal correlation among the propagating paths also increases which consequently reduces the channel capacity and diversity gain. The coupling between antenna elements can be reduced by maintaining a distance of half wavelength. However, due to the need for miniaturization of the antenna, the space between the antenna elements is limited. Parasitic elements [16] and neutralization lines [18] are introduced to improve isolation. Defected ground structures (DGS) are widely used in UWB antennas to improve isolation [4, 5].

In [3], a MIMO antenna uses hybrid Quadric-Koch island fractal geometry, but no isolation techniques are used between the antenna elements, and the antenna occupies a large area. However, as

Received 6 February 2018, Accepted 21 March 2018, Scheduled 4 April 2018
* Corresponding author: Gnanaharan Irene (irenesuriya@gmail.com).
The authors are with the VIT University, Vellore 632014, India.

the distance between the antenna elements is small, the mutual coupling between the antenna elements is less than 17 dB. In [6], a fractal MIMO antenna is proposed with a T-shaped stub placed between the antenna elements to improve the isolation. The isolation obtained is greater than 15 dB, but the coupling between the antenna elements is higher in the lower frequency band. In [7], a MIMO antenna uses Koch fractal geometry at the edges of an octagonal monopole, but the size of the antenna is large. Isolation is improved by placing stubs between the antenna elements, and the isolation obtained is greater than 17 dB. In [8], a UWB antenna with Koch fractal geometry designed on the sides of a hexagonal monopole is proposed. However, band-notch characteristics are not obtained in the above geometry. In [9], a UWB MIMO antenna with Minkowski fractal geometry is proposed. To improve the isolation, an L-shaped stub is introduced between the antenna elements, but the isolation between the antenna elements decreases due to the introduction of a defected ground structure. In [10], an I-shaped slot acting as a defected ground structure is introduced where the size of the antenna is $26 \times 26\,\text{mm}^2$. The isolation between the antenna elements is greater than 15 dB, and the peak gain of the antenna is 4.5 dBi. In [11], an antenna of size $22 \times 26\,\text{mm}^2$ is proposed, and the isolation between the antenna elements is greater than 18 dB. In [12], a square monopole of size $22 \times 36\,\text{mm}^2$ is proposed, and the isolation between the antenna elements is greater than 15 dB. The gain of the antenna is 4 dBi. Compared to the antenna structures in [10–12], the introduction of Koch fractal geometry improves the gain of the antenna, and the isolation between the antenna elements is also improved due to the presence of a defected ground structure in the ground plane.

As the requirement of miniaturized, wideband antennas is increasing, the research is being directed towards fractals [22]. Using fractal geometry in antennas improves the radiation efficiency while keeping the radiation resistance high and the stored reactive energy low [23]. The main advantage of fractal antennas are frequency independent performance. However, the disadvantages of fractal antennas are their complexity. These antennas are highly useful in the military, as they can reduce radar cross section (RCS).

In this paper, a novel compact Koch Fractal UWB MIMO antenna is designed and developed. The antenna band rejects the downlink C-band from 3.7 to 4.2 GHz, the uplink C-band from 5.75 to 6.05 GHz, the meteorological satellite service frequency band from 7.450 to 7.550 GHz for the geostationary satellite services, the meteorological satellite service from 7.750 to 7.9 GHz for the non-geostationary satellite services and the Earth exploration satellite services from 8.025 to 8.4 GHz for the geostationary satellite services. The CST Microwave Studio is used for design and simulations. The simulated results are verified by fabricating the antenna and measuring the results.

The rest of the paper is structured as follows. Section 2 gives the detailed analysis of fractal antennas. The effects of the defected ground and the spiral slot on the UWB MIMO antenna are also discussed in this section. Section 3 discusses the simulated and measured results, and Section 4 concludes the major findings.

2. PROPOSED ANTENNA DESIGN

2.1. Antenna Configuration

The antenna is designed on an FR4 substrate with dimensions $22 \times 32\,\text{mm}^2$ and thickness 1.6 mm. The relative permittivity ε_r of the FR4 substrate is 4.4, and the loss tangent $\tan\delta$ is 0.02 [15]. The proposed UWB-MIMO antenna meets the advantages of the uni-planar antenna. The electromagnetic simulation software, CST Microwave studio was used to design and optimize the antenna structure. The geometry of the inside cut Koch Fractal UWB-MIMO antenna is as shown in Fig. 1. The top layer of the UWB-MIMO antenna which consists of two symmetrically placed Koch fractal hexagonal monopole antenna elements is shown in Fig. 1(a), and the bottom layer which consists of a partial ground with a ring structure which acts as a defected ground structure [10] is shown in Fig. 1(b). The fabricated configurations of the antenna are as shown in Fig. 2. The top layer of the fabricated antenna is as shown in Fig. 2(a), and the bottom layer of the fabricated antenna is as shown in Fig. 2(b). Microstrip line feeding technique is utilized to feed the antenna elements. The parameters of the antenna are given in Table 1.

Koch fractal geometry when being applied to the hexagonal monopole increases the electrical path length. It also decreases the resonant frequency which is a direct function of the limit in the increase

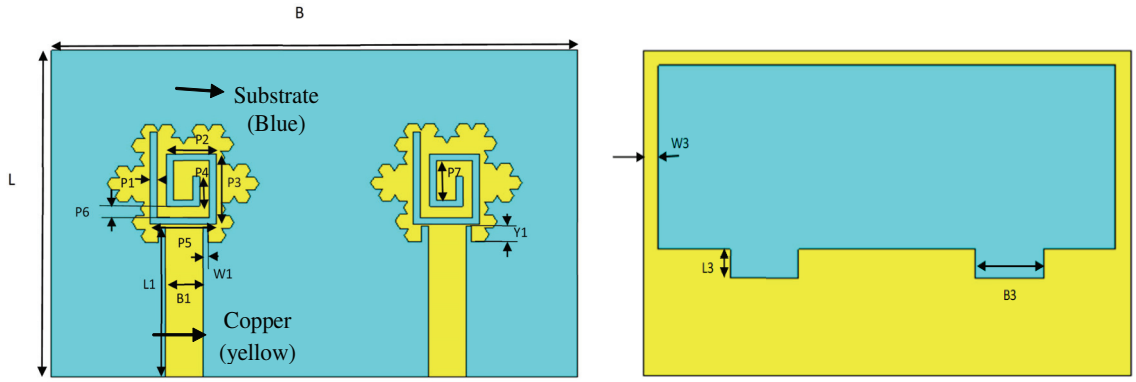

Figure 1. (a) The top and (b) the bottom layer of the proposed UWB-MIMO antenna.

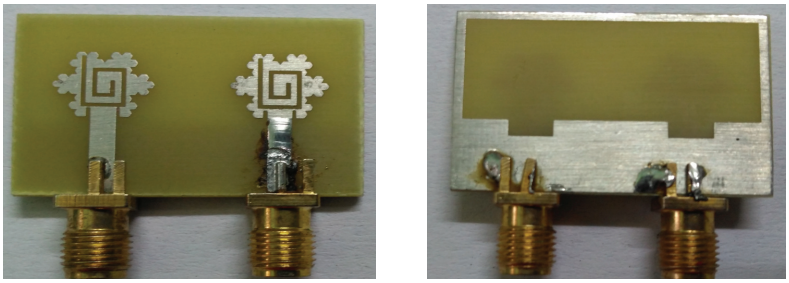

Figure 2. The configuration of the antenna (a) top layer of the substrate and (b) bottom layer of the substrate.

Table 1. Parameters of the designed antenna. All values are in millimeters.

Parameter	Value	Parameter	Value	Parameter	Value	Parameter	Value
L	22	$B2$	5.7	$W3$	1	$P5$	4
B	32	$L3$	2	$P1$	0.4	$P6$	0.8
$L1$	10.4	$B3$	4.5	$P2$	3		
$B1$	2.3	$W1$	0.35	$P3$	4.7		
$L2$	8.6	$Y1$	1.1	$P4$	2		

of the antennas' effective volume [20]. Miniaturization phenomenon [21] and wideband properties are obtained by applying the geometrical principles of Koch fractal to the sides of the hexagonal monopole. Fig. 3 gives the repetitive generation of the Koch fractal geometry. In the first iteration, consider a length of dimension A as shown in Fig. 3(a). In the second iteration, length A is divided into three equal parts, and the middle part is formed as a combination of two equal parts as shown in Fig. 3(b). The third iteration further divides each length A/3 into 3 equal parts as shown in Fig. 3(c). The process is repeated in consecutive iterations. The Koch fractal geometry is placed along the sides of the hexagon, and the iteration is applied to the sides of the hexagon to form the Koch fractal hexagonal monopole till the third iteration.

The S_{11} reflection coefficient obtained as the antenna evolves is as shown in Fig. 4. Using a partial ground plane improves the bandwidth of the antenna, and a rectangular slot is also created in the ground plane to increase the current path and to further widen the bandwidth of the UWB-MIMO antenna. The UWB is obtained by combining the multiple resonances that are formed within the frequency range

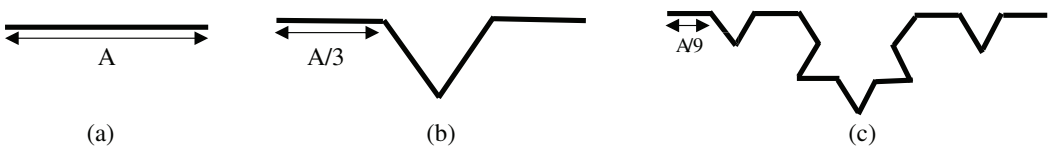

Figure 3. (a) Initializing structure, (b) first iteration and (c) second iteration.

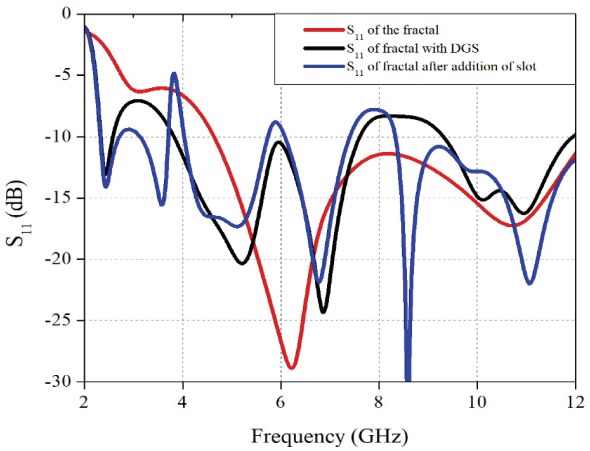

Figure 4. Comparison of the reflection coefficient S_{11} of the fractal antenna with the introduction of ring structure in the ground and the addition of the spiral slot.

from 3.1 to 13.6 GHz. The antenna also resonates in the 2.4 GHz Bluetooth frequency band.

The antenna rejects the C-band downlink frequency from 3.7–4 GHz, the C-band uplink frequency from 5.925–6.25 GHz and the satellite bands from 7.45 to 8.4 GHz. The band 7.45–7.55 GHz is used by the meteorological satellite service for the geostationary satellite services. The band 7.75–7.9 GHz is used by the meteorological satellite service for non-geostationary satellite services. The band 8.025–8.4 GHz is used by the Earth exploration satellites for geostationary satellite services. UWB technology is not compatible with radio astronomy service.

2.2. Effect of Defected Ground Structure

To reduce the mutual coupling between antenna elements, a ring structure is placed in the ground. The ring structure behaves as a defected ground structure, and it reduces the mutual coupling between antenna elements by behaving as a band reject filter.

The main advantages of the defected ground structure are that it is useful in miniaturizing the size of the antenna and improves the bandwidth of the antenna. The bandwidth of the antenna is widened by 0.22% after introduction of the ring structure. The surface current distribution of the antenna with port_1 excited, and the presence of defected ground structure is as shown in Fig. 5. There is cancelling of current at the edges of the spiral slot which leads to introduction of the band notch at the downlink C-band frequency and at the uplink C-band frequency as shown in Fig. 5(a). From Fig. 5(b), the introduction of the partial ground, the defect in the ground and the addition of the ring structure reduce the coupling to the adjacent antenna element.

The surface current distribution at 6.8 GHz is shown in Fig. 5(c), and the surface current distribution at 8.6 GHz is shown in Fig. 5(d). The introduction of the partial ground, the defect in the ground and the ring structure reduce the coupling between the antenna elements.

2.3. Effect of Spiral Slot in the Antenna

The presence of the slot widens the bandwidth of the antenna by 0.15%. It also introduces notches at the C-band downlink frequency and C-band uplink frequency band. The lower frequency of operation

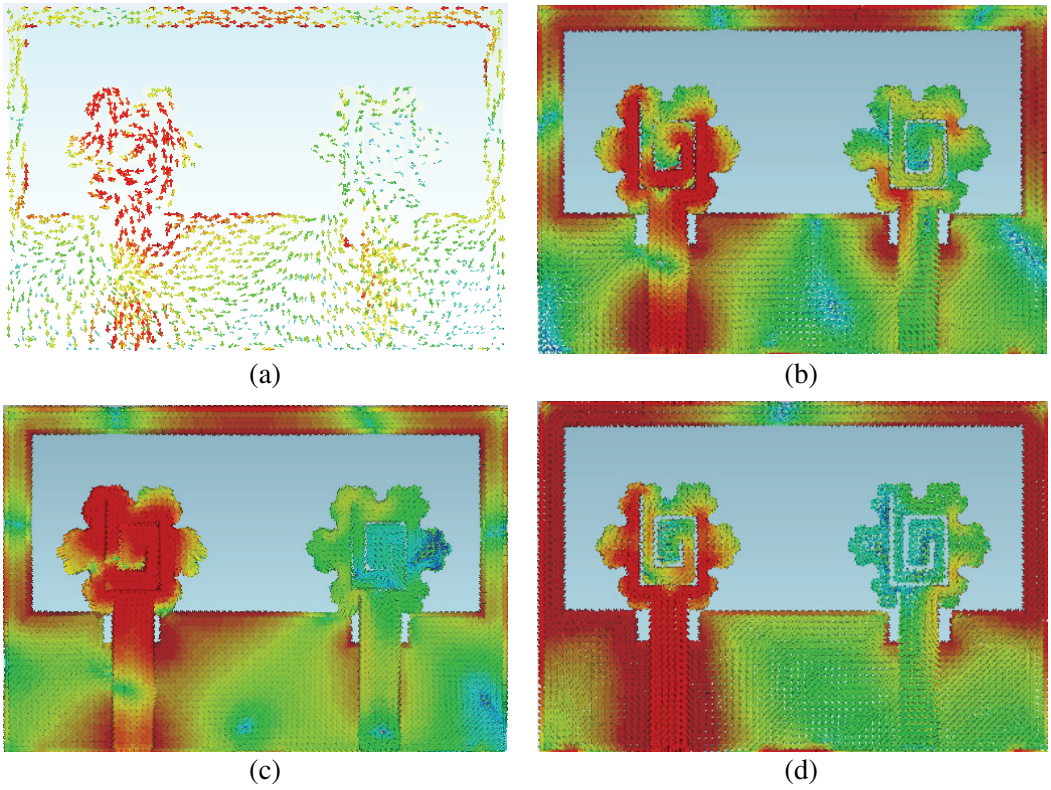

Figure 5. Surface current distribution of the dual element fractal UWB MIMO antenna with port_1 excited at (a) 6.8 GHz to represent the direction of current flow, (b) at 3.6 GHz, (c) at 6.8 GHz and (d) at 8.6 GHz.

of the spiral slot is obtained when the circumference of the spiral and the wavelength are equal

$$f_{lower} = \frac{c}{2\pi R_{spiral}} \tag{1}$$

The upper frequency of operation of the spiral slot is obtained when the inner radius is considered

$$f_{upper} = \frac{c}{4R_o} \tag{2}$$

3. RESULTS AND DISCUSSION

The simulated and measured reflection coefficients, S_{11}, of the antenna are as shown in Fig. 6(a). There is good agreement between the simulated and measured values. The variation of the measured values from the simulated reflection coefficient values is 0.315%. This is because of the losses due to the connector and the losses due to soldering tolerance. The bandwidth of the UWB-MIMO antenna is from 2.3 GHz to 2.7 GHz with a fractional bandwidth of 16% and from 3.1 GHz to 13.6 GHz with a fractional bandwidth of 125%. The S_{11} and S_{22} of the antenna are identical, which shows that the antenna is symmetrical. The resonant frequency bandwidth from 4–5.75 GHz is 35.8%, from 6.05–7.4 GHz is 20%, and from 8.3–13.6 GHz is 48%.

The mutual coupling of the antenna given by S_{21} of the antenna is obtained as less than 19 dB, seen from Fig. 7(b). The S_{12} and S_{21} of the antenna are also identical.

3.1. Equivalent Circuit of the Antenna

Useful insights regarding the performance of the antenna can be obtained from the equivalent circuit using the foster canonical form assuming no ohmic losses. For a UWB antenna, large bandwidth is

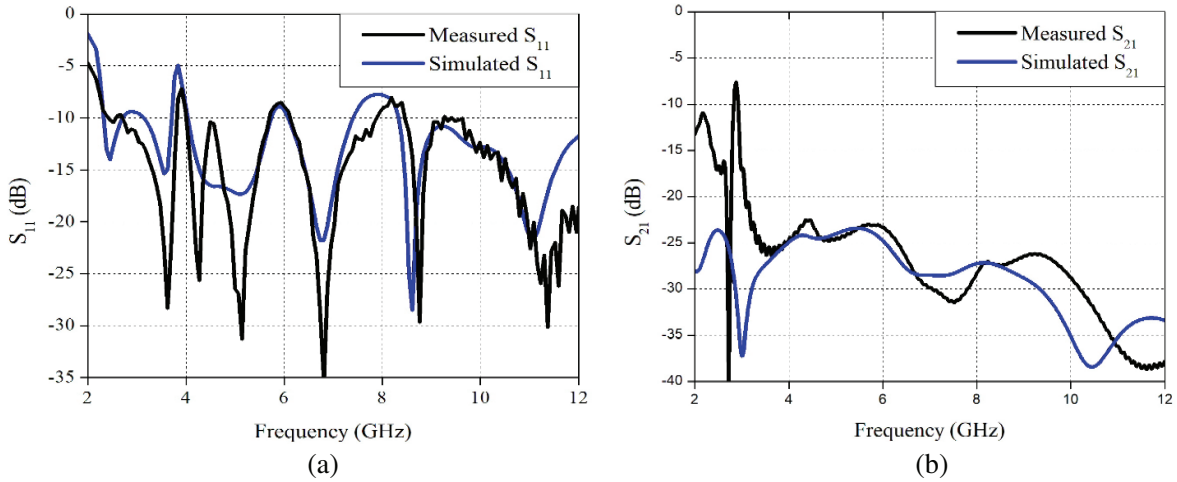

Figure 6. (a) Comparison of the simulated and measured return loss of the antenna and (b) comparison of the simulated and measured isolation of the antenna.

due to the overlapping of several adjacent resonances and can be represented as serially connected parallel RLC circuits [13]. This is obtained by transforming the resonant peaks of the simulated input impedance of reference UWB antenna into the equivalent parallel RLC resonant circuit. C_0 and L_0 account for the static antenna capacitance and probe inductance [13]. The band-notched functions are realised according to conceptual circuit model by connecting the antenna input impedance with either a parallel or a series R-L-C resonant circuit depending on the impedance characteristics at the notched frequency [14]. The real part of the input impedance of S_{11} of the UWB MIMO antenna is shown in Fig. 7(a), and the imaginary part is shown in Fig. 7(b). From the real part of input impedance of S_{11} from Fig. 7(a), it can be seen that the antenna peaks are at 3.5 GHz, 4.1 GHz, 5.3 GHz, 6.3 GHz, 8.2 GHz, 9.3 GHz and at 10.3 GHz in the UWB, and each frequency is represented as a parallel RLC circuit connected in series and the antenna band notches at 3.82 GHz, 5.9 GHz and 7.9 GHz. Each frequency is represented as a series RLC circuit connected in parallel. From the imaginary part of the simulated impedance graph of Fig. 7(b), it can be seen that for the notch bands at 3.82 GHz and 5.9 GHz, the imaginary component crosses zero, changing from capacitive to inductive, and for the notch bands at 7.9 GHz, the imaginary component is inductive with low resistance values, showing similar behavior of a series RLC circuit. Fig. 8 represents the equivalent circuit of the proposed UWB MIMO fractal antenna.

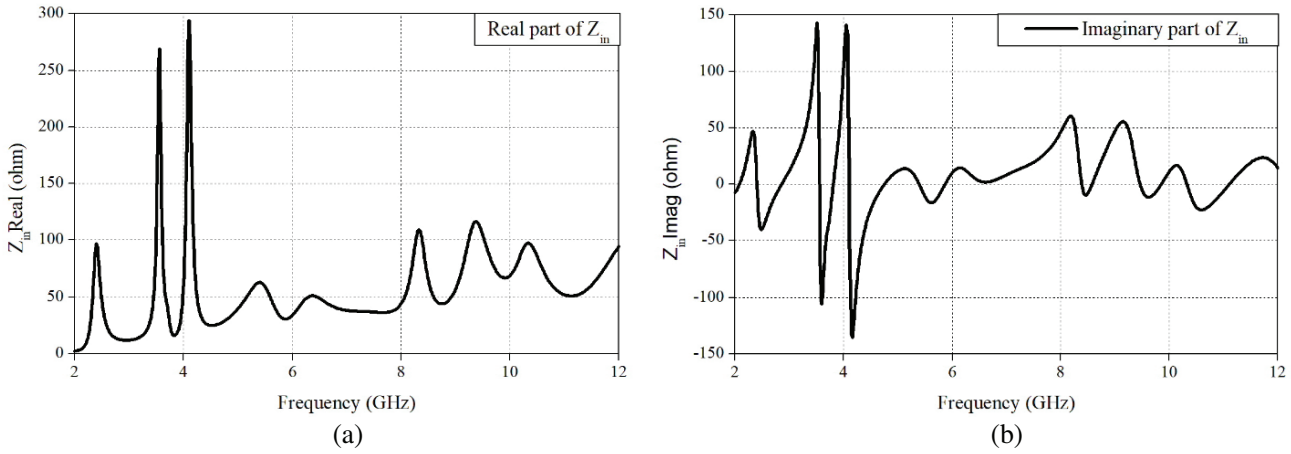

Figure 7. (a) Real part and (b) imaginary part of input impedance of the S_{11} of the antenna.

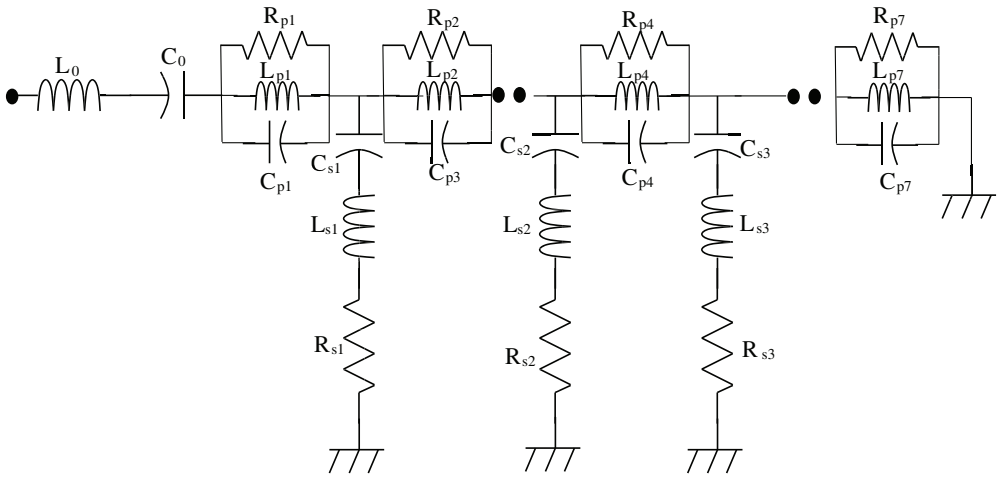

Figure 8. Equivalent circuit of the UWB MIMO fractal antenna.

The parameters of the resistors, capacitors and inductors in the equivalent circuit are as shown in Table 2 and are obtained using Foster canonical forms. The parallel RLC network acts as a band-pass filter, thus creating a resonance, and the series RLC network acts as a band-reject filter, thus rejecting the required frequency. A combination of the series RLC network and the parallel RLC network gives the desired UWB.

Table 2. Element values of the equivalent circuit of the fractal UWB MIMO antenna.

Resonant frequencies								
Frequency (GHz)	3.5	4.1	5.3	6.3	8.2	9.3	10.3	8.6
R_{pn} (Ω)	243.46	282.67	62.962	51.57	112.17	118.68	97.23	16.058
L_{pn} (nH)	0.497	1.165	6.334	7.438	9.293	6.734	4.152	0.129
C_{pn} (pF)	4.089	13.07	1.38	0.84	0.399	0.431		2.6798
Band-notch frequencies								
Frequency (GHz)	3.8	5.9	7.9					
R_{sn} (Ω)	16.058	27.817	42.652					
L_{sn} (nH)	0.093	0.214	8.497	L_0 (nH)	0.63			
C_{sn} (pF)	18.486	0.152	0.475	C_0 (pF)	1.09			

3.2. Radiation Characteristics

The radiation pattern of the antenna at port_1 when port_2 is matched to a 50 Ω load at the frequencies 4.6 GHz, 6.8 GHz and 8.6 GHz is as shown in Fig. 9. The radiation characteristics at 3.6 GHz are as shown in Fig. 9(a), at 6.8 GHz in Fig. 9(b) and at 8.6 GHz in Fig. 9(c). The radiation characteristics are enhanced due to the Koch fractal geometry [19]. The gain of the antenna is improved due to the radiation characteristics of the antenna. The gain of the antenna is as shown in Fig. 10. At the notch band it can be seen that there is a loss in peak gain.

3.3. Diversity Performance

The envelope correlation coefficient (ECC) and diversity gain (DG) are used to characterize the diversity performance of the antenna. ECC is calculated in a uniform propagation environment according to the

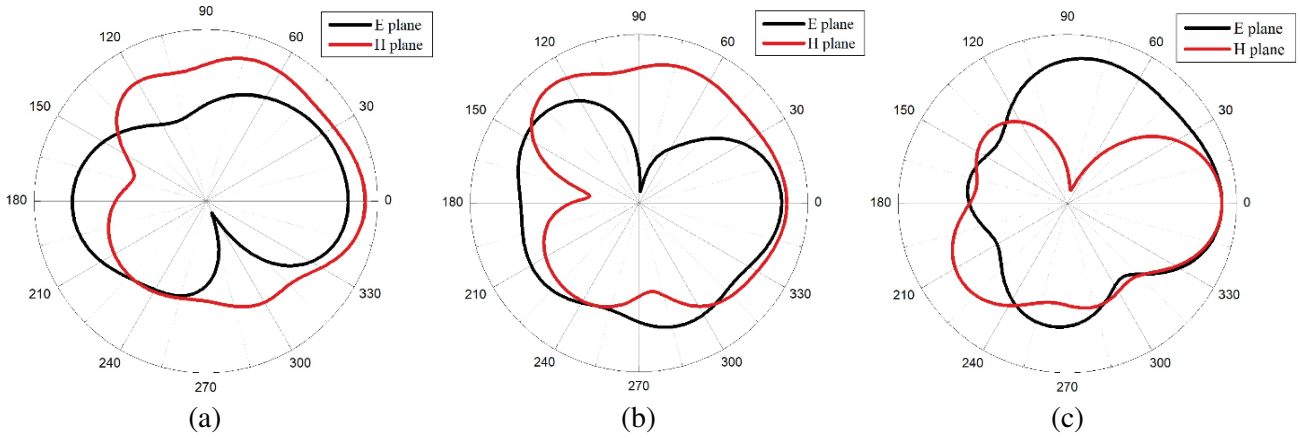

Figure 9. The elevation and azimuth at (a) 4.6 GHz (b) at 6.8 GHz and at (c) 8.6 GHz.

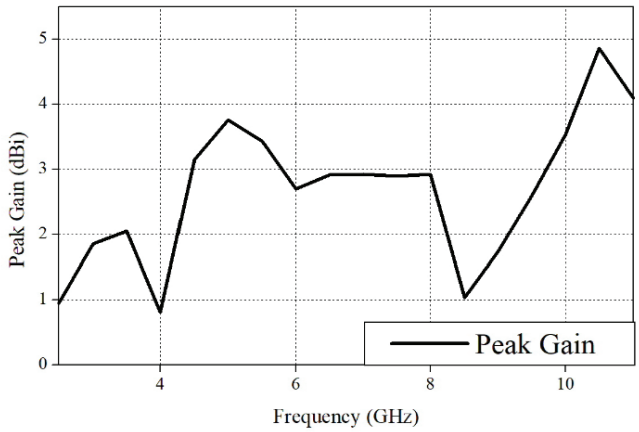

Figure 10. The peak gain of the proposed UWB-MIMO antenna.

given formula [17]

$$\rho_e = \frac{\left|\iint_{4\pi}^{0}\left[\bar{F}1\left(\theta,\varphi\right) * \bar{F}2\left(\theta,\varphi\right)\right] d\Omega\right| 2}{\iint_{4\pi}^{0}\left|\bar{F}1\left(\theta,\varphi\right)\right|^2 d\Omega \iint_{4\pi}^{0}\left|\bar{F}2\left(\theta,\varphi\right)\right|^2 d\Omega} \tag{3}$$

For the antenna to have good diversity performance, the ECC of the antenna should be less than 0.5. The proposed Koch fractal UWB-MIMO antenna satisfies the diversity conditions as its value is less than 0.3 as shown in Fig. 11(a). The value of ECC increases at the notch frequency bands.

In addition, the diversity gain (DG) is greater than 9.8 dB as seen from Fig. 11(b), and its relation with ECC is as follows [4]:

$$DG = \sqrt{1 - ECC^2} \tag{4}$$

The capacity of the channel in a wireless environment is calculated as a function of the radiation characteristics of the antenna elements and the channel environment.

$$C = \log_2\left[det\left(I_N + \frac{\rho}{N} H H^T\right)\right] \tag{5}$$

Correlation between the antenna elements decreases the MIMO capacity, and it induces a capacity loss. For a high SNR, the capacity loss is given by

$$C(Loss) = -\log_2 det\left(\varphi^R\right)$$

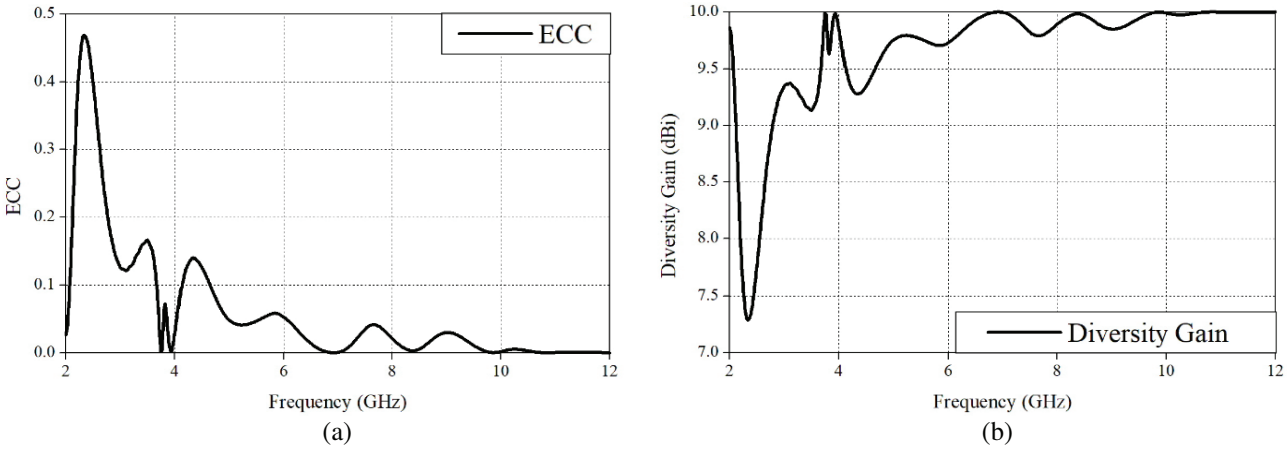

Figure 11. The (a) ECC and (b) diversity gain of the proposed UWB MIMO antenna.

where φ^R is a 2×2 correlation matrix

$$\varphi^R = \begin{bmatrix} \rho_{11} & \rho_{12} \\ \rho_{21} & \rho_{22} \end{bmatrix} \tag{6}$$

where ρ_{ij} is the correlation coefficient between the antennas i and j in an $N \times N$ MIMO antenna. The capacity loss of the antenna is calculated to be 0.256 which is less than the accepted value of 0.4 b/s/Hz. A comparison of the proposed antenna with the UWB MIMO antennas from the literature is given in Table 3.

Table 3. Comparison of the proposed antenna with the antenna's from the literature.

Parameters	**[6]**	**[7]**	**[9]**	**[10]**	**[11]**	**This Work**
Dimensions (mm^2)	20×32	45×45	40×25	48×25	40×25	32×22
Bandwidth (GHz)	3.1 to 7.5	2 to 10.6	3.1 to 10.6	3.1 to 10.6	3.1 to 10.6	3.1 to 13.6
Return loss (dB)	-38	-28	-49	-17	-38	-35
Isolation (dB)	> 15	> 17	> 15	> 20	> 15	> 19
ECC	< 0.06	< 0.005	-	-	< 0.01	< 0.17
Gain (dBi)	-	5	5	-	-	5

4. CONCLUSION

A novel compact miniaturized hexagonal shaped ultra-wideband multiple-input multiple-output (UWB-MIMO) antenna with a Koch fractal monopole is analyzed. The suppression of the inevitable mutual coupling is achieved by using defected ground structures. A spiral shaped slot is introduced on the fractal geometry to widen the impedance bandwidth. The antenna has a better tradeoff in terms of return loss and isolation for the UWB range. In addition, the antenna shows good diversity and gain performance as compared to the UWB MIMO antennas reported in literature.

REFERENCES

1. Jetti, C. R. and V. R. Nandanavanam, "Trident-shape strip loaded dual band-notched UWB MIMO antenna for portable device applications," *AEU-International Journal of Electronics and Communications*, Vol. 83, 11–21, 2018.
2. Rajkumar, S., N. V. Sivaraman, S. Murali, and K. T. Selvan, "Heptaband swastik arm antenna for MIMO applications," *IET Microwaves, Antennas & Propagation*, Vol. 11, No. 9, 1255–1261, 2017.
3. Yadav, A., S. Agarwal, and R. P. Yadav, "SRR and S-shape slot loaded triple band notched UWB antenna," *AEU-International Journal of Electronics and Communications*, Vol. 79, 192–198, 2017.
4. Yang, B. and S. Qu, "A compact integrated Bluetooth UWB dual-band notch antenna for automotive communications," *AEU-International Journal of Electronics and Communications*, Vol. 80, 104–113, 2018.
5. Atallah, H. A., A. B. Abdel-Rahman, K. Yoshitomi, and R. K. Pokharel, "CPW-Fed UWB antenna with sharp and high rejection multiple notched bands using stub loaded meander line resonator," *AEU-International Journal of Electronics and Communications*, Vol. 83, 22–31, 2018.
6. Rajkumar, S., K. T. Selvan, and P. H. Rao, "Compact two-element UWB fractal monopole MIMO antenna using T-shaped reflecting stub for high isolation," *IEEE MTT-S International Microwave and RF Conference*, 348–351, 2015.
7. Tripathi, S., A. Mohan, and S. Yadav, "A compact Koch fractal UWB MIMO antenna with WLAN band-rejection," *IEEE Antennas and Wireless Propagation Letters*, Vol. 14, 1565–1568, 2015.
8. Tripathi, S., A. Mohan, and S. Yadav, "Hexagonal fractal ultra-wideband antenna using Koch geometry with bandwidth enhancement," *IET Microwaves, Antennas & Propagation*, Vol. 8, No. 15, 1445–1450, 2014.
9. Tripathi, S., A. Mohan, and S. Yadav, "A compact octagonal shaped fractal UWB MIMO antenna with 5.5 GHz band-notch characteristics," *IEEE International Microwave and RF Conference (IMaRC)*, 178–181, IEEE, 2014.
10. Zhang, J.-Y., F. Zhang, W.-P. Tian, and Y.-L. Luo, "ACS-fed UWB-MIMO antenna with shared radiator," *Electronics Letters*, Vol. 51, No. 17, 1301–1302, 2015.
11. Luo, C.-M., J.-S. Hong, and L.-L. Zhong, "Isolation enhancement of a very compact UWB-MIMO slot antenna with two defected ground structures," *IEEE Antennas and Wireless Propagation Letters*, Vol. 14, 1766–1769, 2015.
12. Liu, L., S. W. Cheung, and T. I. Yuk, "Compact MIMO antenna for portable UWB applications with band-notched characteristic," *IEEE Transactions on Antennas and Propagation*, Vol. 63, No. 5, 1917–1924, 2015.
13. Pele, I., A. Chousseaud, and S. Toutain, "Simultaneous modeling of impedance and radiation pattern antenna for UWB pulse modulation," *Antennas and Propagation Society International Symposium*, Vol. 2, 1871–1874, IEEE, 2004.
14. Zhou, H.-J., B.-H. Sun, Q.-Z. Liu, and J.-Y. Deng, "Implementation and investigation of U-shaped aperture UWB antenna with dual band-notched characteristics," *Electronics Letters*, Vol. 44, No. 24, 1387–1388, 2008.
15. Mewara, H. S., D. Jhanwar, M. M. Sharma, and J. K. Deegwal, "A printed monopole ellipzoidal UWB antenna with four band rejection characteristics," *AEU-International Journal of Electronics and Communications*, Vol. 83, 222–232, 2018.
16. Khan, M. S., A.-D. Capobianco, A. I. Najam, I. Shoaib, E. Autizi, and M. F. Shafique, "Compact ultra-wideband diversity antenna with a floating parasitic digitated decoupling structure," *IET Microwaves, Antennas & Propagation*, Vol. 8, No. 10, 747–753, 2014.
17. Gulam Nabi Alsath, M. and M. Kanagasabai, "Compact UWB monopole antenna for automotive communications," *IEEE Transactions on Antennas and Propagation*, Vol. 63, No. 9, 4204–4208, 2015.
18. Yu, Y., X. Liu, Z. Gu, and L. Yi, "A compact printed monopole array with neutralization line for UWB applications," *IEEE International Symposium on Antennas and Propagation (APSURSI)*, 1779–1780, 2016.

19. Puente, C., J. Romeu, R. Pous, J. Ramis, and A. Hijazo, "Small but long Koch fractal monopole," *Electronics Letters*, Vol. 34, No. 1, 9–10, 1998.
20. Best, S. R., "On the performance properties of the Koch fractal and other bent wire monopoles," *IEEE Transactions on Antennas and Propagation*, Vol. 51, No. 6, 1292–1300, 2003.
21. Anagnostou, D. E., J. Papapolymerou, C. G. Christodoulou, and M. Tentzeris, "A small planar log-periodic Koch-dipole antenna (LPKDA)," *IEEE Antennas and Propagation Society International Symposium*, 3685–3688, 2006.
22. Anagnostou, D., M. T. Chryssomallis, J. C. Lyke, and C. G. Christodoulou, "A CPW koch dipole slot antenna," *IEEE Topical Conference on Wireless Communication Technology*, 337, 2003.
23. Best, S. R., "On the resonant properties of the Koch fractal and other wire monopole antennas," *IEEE Antennas and Wireless Propagation Letters*, Vol. 1, No. 1, 74–76, 2002.